Analytical solution of the induced currents in multilayer cylindrical conductors under external electromagnetic sources

Jesús Acero[1], Claudio Carretero[2], Ignacio Lope[3], Rafael Alonso[2], José Miguel Burdío[1]

[1] *Departamento de Ingeniera Electrónica y Comunicaciones, Universidad de Zaragoza, 50018 Zaragoza, Spain.*
[2] *Departamento de Física Aplicada, Universidad de Zaragoza, 50009 Zaragoza, Spain.*
[3] *B/S/H/ Home Appliances, 50016 Zaragoza, Spain.*

Corresponding author: Jesús Acero: jacero@unizar.es

Abstract

We present a closed-form solution for the induced losses in round conductors consisting of several concentric layers. The geometry under study corresponds to an infinitely-long and isolated multilayer cylinder where layers can have different electromagnetic properties and the number of layers is not restricted. The multilayer conductor is under an external time-varying magnetic field which induces currents and, accordingly, generates Joule dissipation. Total induced losses are obtained by integrating the losses of each layer. Mathematical expressions of the current distribution in each layer are derived from the solution of Maxwells equations. These expressions consist of a combination of Bessel functions of different kinds and orders. The current distribution in a particular layer not only depends on the properties of the layer but also on the properties of the rest of layers. Consequently, matrix formalism is adopted for describing current distribution of layers. Matrix description is numerically solved and results are compared with finite element simulations for different arrangements and cases.

Keywords: `Closed-form solutions; eddy currents; electromagnetic analysis; skin effect; proximity effect; multilayer structures`

1. Introduction

Tubular conductors are used in many applications at medium-high frequencies, ranging from several kHz up to tens of MHz, in order to alleviate the ac losses, caused by skin and proximity effects. Some popular applications of tubular conductors are induction furnaces or magnetic elements for broadcasting or radio-frequency systems. Apart from the loss reduction, tubular conductors also possess convenient mechanical and thermal properties. Considering induction furnaces, inductors made of copper tubes can adapt to the shape of the work-piece without including bobbins or holders. Moreover, hollow tubes can be cooled by circulating a coolant element, and the operation temperature of bare copper conductors is higher than the temperature limit of insulated magnet wires. These properties make copper tubular conductors potentially attractive for other closely-related applications in the mid-power range, such as wireless power transfer (WPT) systems.

Modeling ac losses in tubular conductors has been addressed by several authors. Dwight proposed several ac loss models for tubes and other shapes mainly based on the solution of the current density in the conductor. In general, his works described approximate solutions mainly based on asymptotic tendencies at both low and high frequencies [1–5] .

Similarly, Arnold developed an approximate solution based on Dwight's results [6]. This work was mainly focused on the study of copper-clad or aluminum-clad (bimetallic) conductors. Schelkunoff studied the case of the coaxial transmission line and developed an exact formula for the internal impedance of a tubular conductor in terms of modified Bessel functions [7]. Teare and Webb proposed a model of the skin effect of solid conductors consisting of several materials, in this case a bimetallic arrangement [8]. This study addressed the case of hollow conductors but an analysis of the loss induced by an external magnetic field was not provided. The diffusion of fields in concentric rods of different prop-

erties was also studied in [9]. Clogston introduced the idea of using multi-layer structures in order to reduce the skin effect and proposed a theory for laminated planar transmission lines [10]. Other authors extended this concept to coaxial lines with the purpose of loss reduction [11]. The current density of cylindrical shells due to axial currents was obtained by solving Maxwells equations through the magnetic vector potential and boundary conditions [12]. The methodology followed in this reference has been applied in the study presented in this paper.

More recently, some authors have proposed numerical solutions for the ac losses in tubular conductors mainly oriented to overcoming the convergence problems of Bessel functions for large arguments [13–17]. Moreover, cylindrical conductors arranged with multiple concentric layers have been proposed to reduce the skin effect of litz wires [18] and the skin effect in inhomogeneous conductors has been also studied [19]. Therefore, interest in this kind of conductors is currently observed.

Despite the substantial number of works on electromagnetic fields involving tubular conductors, it seems that there is still more to contribute in relation to multilayer round conductors, which is the main objective of this paper. This study could be also useful for predicting the losses due to the so called skin and proximity effects.

The remainder of the paper is organized as follows. The conditions assumed in this analysis are presented in Section II. In Section III the impedance of a multilayer round conductor under a longitudinal alternating voltage is derived. Section IV is focused on obtaining fields and losses in a multilayer round conductor in a transverse varying magnetic field. Section V describes the validation of the analytic model by means of FEA simulations for different cases. Finally, Section VI summarizes the contributions of the present work.

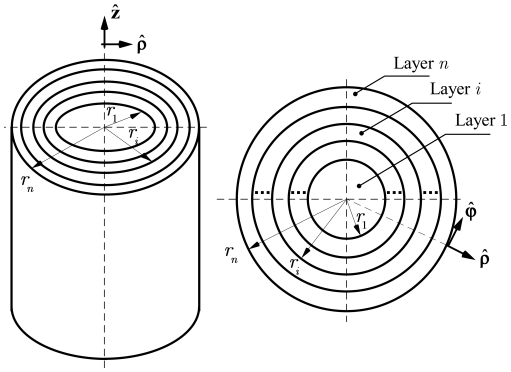

Figure 1: Geometry of a multilayer cylindrical conductor.

2. Conditions of the study and fundamental field equations

The analysis of power induced currents in multi-layer round conductors is carried out adopting the following assumptions. First, a single conductor is considered in order to simplify the analysis. The conductor is an infinitely-long isolated cylinder and curvature in the longitudinal direction is not considered. Second, the conductor consists of concentric layers of a linear, homogeneous and isotropic material. The properties of the ith layer are $\sigma_i, \mu_i, \varepsilon_i$ and its external radius is r_i, as shown in Fig. 1. Third, an external harmonic ($e^{j\omega t}$ time dependence) electromagnetic field is applied and the effect of the field in the conductor and the sources of the field are decoupled. Fourth, the magneto-quasistatic approach (MQS) is assumed in this analysis. At the frequency range of interest of the mentioned applications (from dc to several MHz) the diffusion of the fields inside the conductor dominates the radiation, or equivalently, the displacement current in the system can be neglected compared to the induced currents in the conductor [20]. Considering the preceding assumptions, the electromagnetic field of the system can be described by the following magnetic vector potential equation:

$$\nabla^2 \mathbf{A} + k^2 \mathbf{A} = 0 \tag{1}$$

where k is the wave number and $\mathbf{A}$ is the magnetic vector potential. The wave

number is defined as:

$$k = \sqrt{-j\omega\mu\sigma} \tag{2}$$

and ω is the angular frequency of the harmonic fields. For this geometry, it is convenient to consider the Laplacian in the usual cylindrical coordinate system:

$$\begin{aligned} \nabla^2\mathbf{A} = &\left[\nabla^2 A_\rho - \tfrac{2}{\rho^2}\partial_\varphi A_\varphi - \tfrac{A_\rho}{\rho^2}\right]\hat{\boldsymbol{\rho}} \\ &+ \left[\nabla^2 A_\varphi - \tfrac{2}{\rho^2}\partial_\varphi A_\rho - \tfrac{A_\varphi}{\rho^2}\right]\hat{\boldsymbol{\varphi}} + \nabla^2 A_z\hat{\mathbf{z}} \end{aligned} \tag{3}$$

where

$$\nabla^2 A_\alpha = \frac{1}{\rho}\partial_\rho\left(\rho\partial_\rho A_\alpha\right) + \frac{1}{\rho^2}\partial_\varphi^2 A_\alpha + \partial_z^2 A_\alpha \qquad \alpha{=}\rho,\varphi,z \tag{4}$$

Taking into account that the skin and proximity effects can be derived from the zeroth and first order terms of the transversal magnetic (TM) mode of the electromagnetic field [21], the ac losses can be completely described by the longitudinal component of the vector potential A_z. Moreover, assuming uniform fields along the axial direction of the conductor, i.e. $\partial_z A_z = 0$ and combining these results with (1), the equation to be solved is:

$$\frac{\partial_\rho\left(\rho\partial_\rho A_z\right)}{\rho} + \frac{1}{\rho^2}\partial_\varphi^2 A_z + k^2 A_z = 0 \tag{5}$$

The vector potential in each layer is obtained by applying boundary conditions in the interface between contiguous layers. In this case the boundary conditions represent the continuity of transversal electric and magnetic fields, which in terms of the vector potential is expressed as follows:

$$\begin{aligned} A_{z,i}\left(\rho = r_i\right) &= A_{z,i+1}\left(\rho = r_i\right) \\ \tfrac{1}{\mu_i}\partial_\rho A_{z,i}\left(\rho = r_i\right) &= \tfrac{1}{\mu_{i+1}}\partial_\rho A_{z,i+1}\left(\rho = r_i\right) \end{aligned} \tag{6}$$

where $A_{z,i}$ is the vector potential in the ith layer. For layers with identical magnetic permeability, the boundary conditions impose continuity of both the vector potential and its derivative. Both skin and proximity effects in the multilayer conductor can be described by means of (5) with additional constraints, as is described below.

Apart from these field equations, other fundamental electromagnetic expressions are required in order to calculate the induced currents in the conductor, which is the objective of this work. The first expression corresponds to the relation between the electric field and the vector potential:

$$\mathbf{E} = -j\omega\mathbf{A}, \tag{7}$$

the second is the definition of the voltage in terms of the electric field:

$$V = -\oint \mathbf{E} \cdot d\mathbf{l}, \tag{8}$$

and the third is the relation between the current density in a conductor of conductivity σ and the electric field:

$$\mathbf{J} = \sigma\mathbf{E}. \tag{9}$$

3. Field solution of the skin effect

The governing equation of the skin effect in a multilayer conductor is (5) by imposing the condition $\partial_\varphi^2 A_z = 0$ which captures the axial symmetry of the current density [22]. Therefore:

$$\frac{\partial_\rho \left(\rho \partial_\rho A_z\right)}{\rho} - j\omega\mu\sigma A_z = 0 \tag{10}$$

For the ith layer the solution of this equation is [22]:

$$A_{z,i} = C_i J_0\left(k_i\rho\right) + D_i Y_0\left(k_i\rho\right) \qquad r_{i-1} < \rho < r_i \tag{11}$$

where J_0 and Y_0 are Bessel functions of the first and the second kind of order zero, respectively. Moreover:

$$k_i = \sqrt{-j\omega\mu_i\sigma_i} = \frac{-1+j}{\delta_i} \tag{12}$$

with δ_i being the classical skin depth of the fields in the ith layer. For convenience, the parameter ξ_i is also defined:

$$\xi_i = \sqrt{\omega \mu_i \sigma_i} \Rightarrow k_i = \sqrt{-j}\xi_i \tag{13}$$

Substituting (11) in (6) it follows that:

$$\mathbf{M}_{i+1}\left(k_{i+1}, r_i\right) \cdot \begin{bmatrix} C_{i+1} \\ D_{i+1} \end{bmatrix} = \mathbf{M}_i\left(k_i, r_i\right) \cdot \begin{bmatrix} C_i \\ D_i \end{bmatrix} \tag{14}$$

and also considering the derivatives of Bessel functions [23], the matrix $\mathbf{M}_i$ is defined as follows:

$$\mathbf{M}_i\left(k_i, r_i\right) = \begin{bmatrix} J_0\left(k_i r_i\right) & Y_0\left(k_i r_i\right) \\ \frac{k_i}{\mu_i} J_1\left(k_i r_i\right) & \frac{k_i}{\mu_i} Y_1\left(k_i r_i\right) \end{bmatrix} \tag{15}$$

Therefore, the coefficients of two consecutive layers are connected as follows:

$$\begin{bmatrix} C_{i+1} \\ D_{i+1} \end{bmatrix} = \mathbf{R}_{i+1,i}\left(k_{i+1}, k_i, r_i\right) \cdot \begin{bmatrix} C_i \\ D_i \end{bmatrix} \tag{16}$$

where $\mathbf{R}_{i+1,i}\left(k_{i+1}, k_i, r_i\right)$ has the following expression:

$$\mathbf{R}_{i+1,i}\left(k_{i+1}, k_i, r_i\right) = \frac{1}{K_{R_{i+1,i}}} \times \begin{bmatrix} R^{11}_{i+1,i} & R^{12}_{i+1,i} \\ R^{21}_{i+1,i} & R^{22}_{i+1,i} \end{bmatrix} \tag{17}$$

and parameters $K_{Ri+1,i}, R^{11}_{i+1,i}, R^{12}_{i+1,i}, R^{21}_{i+1,i}, R^{22}_{i+1,i}$ are defined in the Appendix A.

The cases of the first and last layer coefficients of (11) require special treatment. On the one hand, considering that in the first layer the vector potential must be bounded and also considering the characteristics of Bessel functions, it follows that $D_1 = 0$. Therefore, recursively applying (16), an equation connecting the coefficients of a particular layer can be found:

$$\begin{bmatrix} C_{i+1} \\ D_{i+1} \end{bmatrix} = \prod_{j=i}^{1} \mathbf{R}_{j+1,j}\left(k_{j+1}, k_j, r_j\right) \cdot \begin{bmatrix} C_1 \\ 0 \end{bmatrix} \tag{18}$$

On the other hand, the coefficients of the last layer are related with the voltage V per unit of length applied to the conductor by using the expressions (7) and (8):

$$-j\omega A_{z,n}\left(\rho = r_n\right) = -V/l \tag{19}$$

Therefore

$$\left[\begin{array}{cc} J_0\left(k_n r_n\right) & Y_0\left(k_n r_n\right) \end{array}\right] \cdot \left[\begin{array}{c} C_n \\ D_n \end{array}\right] = \frac{1}{j\omega} \cdot \frac{V}{l} \tag{20}$$

And this equation combined with (18) gives:

$$\left[\begin{array}{cc} J_0\left(k_n r_n\right) & Y_0\left(k_n r_n\right) \end{array}\right] \cdot \prod_{j=n-1}^{1} \mathbf{R}_{j+1,j}\left(k_{j+1}, k_j, r_j\right) \cdot \left[\begin{array}{c} C_1 \\ 0 \end{array}\right] = \frac{1}{j\omega} \cdot \frac{V}{l} \tag{21}$$

This equation allows the coefficient C_1 to be calculated and for the rest of the layers the coefficients can be calculated by (16).

Next, the internal impedance of the conductor is derived. According to the relation between the magnetic vector potential and the current density, the current in the ith layer is:

$$I_i = \left(-j\omega\sigma_i\right) \cdot 2\pi \int_{r_{i-1}}^{r_i} \left(C_i J_0\left(k_i\rho\right) + D_i Y_0\left(k_i\rho\right)\right)\rho d\rho \tag{22}$$

The solutions of integrals with Bessel functions are [23]

$$\int uB_0\left(u\right) \cdot du = u \cdot B_1\left(u\right) \qquad B_n = J_n, Y_n \tag{23}$$

Therefore, the current in the ith layer is:

$$\begin{aligned} I_i = \left(-j\omega\sigma_i\right) \cdot 2\pi \left[C_i \cdot \left(r_i J_1\left(k_i r_i\right) - r_{i-1} J_1\left(k_i r_{i-1}\right)\right) + \right. \\ \left. D_i \cdot \left(r_i Y_1\left(k_i r_i\right) - r_{i-1} Y_1\left(k_i r_{i-1}\right)\right)\right] \end{aligned} \tag{24}$$

The total current in the conductor is given by:

$$I = \sum_{i=1}^{n} I_i \tag{25}$$

and therefore the internal impedance per unit of length is:

$$Z_{cond} = \frac{V/l}{I} = R_{cond} + j\omega L_{cond} \tag{26}$$

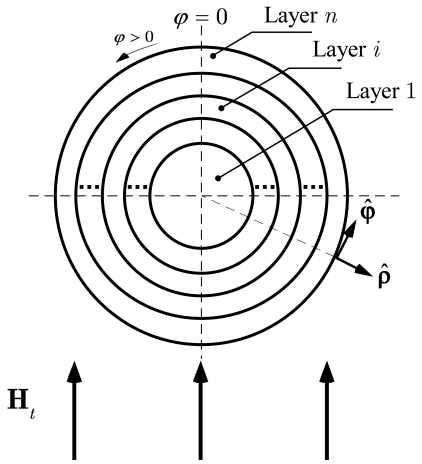

Figure 2: Multilayer cylindrical conductor under a uniform transverse magnetic field.

The real part of Z_{cond} corresponds to the conductor resistance, whereas the imaginary part corresponds to the internal inductance of the conductor.

Usually it is useful to quantify the increase of the resistance of a conductor due to the frequency of the applied voltage with respec to its dc resistance. This increase is the so called *skin resistance*, R_{skin}, because it is caused by the skin effect. In order to obtain R_{skin} the dc resistance is required:

$$R_{dc} = \left(\pi \sum_{i=1}^{n} \sigma_i \left(r_i^2 - r_{i-1}^2 \right) \right)^{-1} \qquad \text{with} \quad r_0 = 0 \tag{27}$$

Therefore, the skin resistance is:

$$R_{skin} = {}^{R_{cond}}/_{R_{dc}} \tag{28}$$

4. Induced losses in multilayer cylindrical conductor under a transverse alternanting magnetic field

4.1. Field solution

The TM-mode of the electromagnetic field in the conductor includes the contribution of a transverse uniform magnetic field $\mathbf{H}_t$, which is the origin of

the induced losses [21]. The conductor and the applied field are shown in Fig. 2. Considering (5), the condition to obtain the equation describing the induced losses is $\partial_{\varphi}^{2} A_z = -A_z$ [22]. Physically this condition arises from the fact that the total induced current in the conductor under a transverse uniform magnetic field must be zero, or in other words, the induced current density presents odd parity. As a consequence, A_z also exhibits odd parity with respect to the φ coordinate. In this case, (5) reduces to:

$$\frac{\partial_{\rho}\left(\rho \partial_{\rho} A_z\right)}{\rho} - \left(\frac{1}{\rho^2} + j\omega\mu\sigma\right) A_z = 0 \tag{29}$$

Inside the conductor, the solution of the preceding equation for the ith layer can be written as follows [22]:

$$A_{z,i} = \left(F_i I_1\left(\kappa_i \rho\right) + G_i K_1\left(\kappa_i \rho\right)\right) \sin\varphi \qquad r_{i-1} < \rho < r_i \tag{30}$$

where the odd parity of $A_{z,i}$ is taken into account by means of the sine function. Moreover:

$$\kappa_i = j k_i = \sqrt{j\omega\mu_i\sigma_i} = -\frac{1+j}{\delta_i} \tag{31}$$

Outside the conductor, the solution of (29) is [22]:

$$A_z = \left(C'\rho + D'/\rho\right) \sin\varphi \qquad \rho > r_n \tag{32}$$

Functions I_1 and K_1 of (30) are modified Bessel functions [23] of the first and the second kind of order one, respectively. In this case, this kind of solution is convenient because these functions I_1 and K_1 can be rewritten in terms of Kelvin functions [23], which allows the power dissipation to be calculated in the conductor.

In order to apply the boundary conditions (6), the derivative of the potential vector is required. This derivative can be obtained by using the tables given in [23].

$$\begin{array}{ll} \partial_\rho A_{z,i} = \left\{ F_i \cdot \left(-\frac{1}{\rho} I_1 \left(\kappa_i \rho \right) + \kappa_i I_0 \left(\kappa_i \rho \right) \right) + \right. & \\ \left. G_i \cdot \left(\frac{1}{\rho} K_1 \left(\kappa_i \rho \right) + \kappa_i K_0 \left(\kappa_i \rho \right) \right) \right\} \cdot \sin\varphi & r_{i-1} < \rho < r_i \\ \partial_\rho A_z = \left(C' - \frac{D'}{\rho^2} \right) \cdot \sin\varphi & \rho > r_n \end{array} \tag{33}$$

A procedure similar to that followed in the previous section is adopted to obtain the solutions of (30) and (32). Considering two adjacent layers, and substituting (30) in (6), it follows that:

$$\mathbf{N_{i+1}} \left(\kappa_{i+1}, r_i \right) \cdot \begin{bmatrix} F_{i+1} \\ G_{i+1} \end{bmatrix} = \mathbf{N_i} \left(\kappa_i, r_i \right) \cdot \begin{bmatrix} F_i \\ G_i \end{bmatrix} \tag{34}$$

where:

$$\mathbf{N_i} \left(\kappa_i, r_i \right) = \begin{bmatrix} I_1 \left(\kappa_i r_i \right) & K_1 \left(\kappa_i r_i \right) \\ \frac{1}{\mu_i} \left(-\frac{1}{r_i} I_1 \left(\kappa_i r_i \right) + \kappa_i I_0 \left(\kappa_i r_i \right) \right) & \frac{1}{\mu_i} \left(\frac{1}{r_i} K_1 \left(\kappa_i r_i \right) + \kappa_i K_0 \left(\kappa_i r_i \right) \right) \end{bmatrix} \tag{35}$$

In this expression I_0 and K_0 are modified Bessel functions of the first and second kind and order zero. Therefore, following the procedure of the previous section, the coefficients of two consecutive layers are connected by means of:

$$\mathbf{S}_{i+1,i} \left(\kappa_{i+1}, \kappa_i, r_i \right) = \frac{1}{K_{S\,i+1,i}} \times \frac{1}{\mu_i} \times \begin{bmatrix} S^{11}_{i+1,i} & S^{12}_{i+1,i} \\ S^{21}_{i+1,i} & S^{22}_{i+1,i} \end{bmatrix} \tag{36}$$

where parameters $K_{S\,i+1,i}, S^{11}_{i+1,i}, S^{12}_{i+1,i}, S^{21}_{i+1,i}, S^{22}_{i+1,i}$ are defined in the Appendix A.

As occurs in the previous section, the coefficient G_1 is zero taking into account the properties of Bessel functions and also considering that in the first layer the field must be bounded. Moreover, an expression relating the coefficients of the last layer, which involves the applied field $\mathbf{H}_t$ can be obtained as follows. On the one hand, applying the boundary conditions of (6) to the nth layer, the following conditions are obtained:

$$\begin{bmatrix} I_1(\kappa_n r_n) & K_1(\kappa_n r_n) \\ \frac{1}{\mu_n}\left(-\frac{1}{r_n}I_1(\kappa_n r_n)+\kappa_n I_0(\kappa_n r_n)\right) & \frac{1}{\mu_n}\left(\frac{1}{r_n}K_1(\kappa_n r_n)+\kappa_n K_0(\kappa_n r_n)\right) \end{bmatrix} \times \begin{bmatrix} F_n \\ G_n \end{bmatrix} = \begin{bmatrix} r_n & \frac{1}{r_n} \\ \frac{1}{\mu_0} & -\frac{1}{\mu_0}\frac{1}{r_n^2} \end{bmatrix} \begin{bmatrix} C' \\ D' \end{bmatrix} \tag{37}$$

On the other hand, far from the conductor the field tends to be equal to the applied transverse magnetic field $\mathbf{H}_t$ because the influence of the conductor can be neglected. Considering that the magnetic field can be obtained from the vector potential, i.e.:

$$\mathbf{H} = \frac{1}{\mu}\nabla \times \mathbf{A} = \frac{1}{\rho}\frac{\partial_\varphi A_z}{\mu}\hat{\boldsymbol{\rho}} - \frac{\partial_\rho A_z}{\mu}\hat{\boldsymbol{\varphi}} \tag{38}$$

Therefore, considering the expression of the vector potential outside the conductor (32) and applying the condition ($\rho \to \infty$) and also applying the characteristics of the unit vectors $\hat{\boldsymbol{\rho}}$ and $\hat{\boldsymbol{\varphi}}$ and considering the reference $\varphi = 0$ shown in Fig. 2, it follows that:

$$C' = \mu_0 H_t \tag{39}$$

Therefore the following equation is obtained:

$$\frac{1}{\mu_n}\begin{bmatrix} \mu_n I_1(\kappa_n r_n) & \mu_n K_1(\kappa_n r_n) \\ \left(-\frac{1}{r_n}I_1(\kappa_n r_n)+\kappa_n I_0(\kappa_n r_n)\right) & \left(\frac{1}{r_n}K_1(\kappa_n r_n)+\kappa_n K_0(\kappa_n r_n)\right) \end{bmatrix} \times \prod_{j=n-1}^{1} \mathbf{S}_{j+1,j}(\kappa_{j+1},\kappa_j,r_j) \cdot \begin{bmatrix} F_1 \\ 0 \end{bmatrix} = \begin{bmatrix} r_n & \frac{1}{r_n} \\ \frac{1}{\mu_0} & -\frac{1}{\mu_0}\frac{1}{r_n^2} \end{bmatrix} \begin{bmatrix} \mu_0 H_t \\ D' \end{bmatrix} \tag{40}$$

Coefficients F_1 and D' are obtained by solving the preceding equation system. This equation is numerically solved by means of a MATLAB code. Moreover, the rest of the coefficients can be obtained with F_1 and (36). Currents and fields in layers can be obtained by applying the relationships between these magnitudes and the vector potential.

4.2. CALCULATION OF POWER DISSIPATION

The power dissipated in the conductor is generated by the induced currents due to the transverse harmonic magnetic field $\mathbf{H}_t$. Part of the energy of the magnetic field is being transferred into the conductor. This power can be calculated by integrating the Joule's losses generated by the induced currents in the conductor. The total Joule's losses can be calculated by adding the Joule's losses in each layer. Assuming harmonic dependency, the induced losses in the ith layer are given by:

$$P_{\text{ind},i} = \frac{1}{2}\int_V \mathbf{E}_i \cdot \mathbf{J}_i^* dV = \frac{\sigma_i}{2}\int_V |E_i|^2 dV = \frac{\omega^2\sigma_i}{2}\int_V |A_i|^2 dV \tag{41}$$

where $\mathbf{E}_i, \mathbf{J}_i$ are the electric field and the current density in the ith layer, and the asterisk represents the conjugated magnitude. Moreover, also considering that the vector potential in each layer is given by (30), the induced losses in each layer can be calculated by solving the following integral:

$$\begin{aligned} &P_{\text{ind},i} = \tfrac{\omega^2\sigma_i}{2}\int_0^{2\pi}\sin^2\varphi d\varphi \\ &\times\int_{r_{i-1}}^{r_i}\left(F_i I_1\left(\kappa_i\rho\right) + G_i K_1\left(\kappa_i\rho\right)\right)\cdot\left(F_i I_1\left(\kappa_i\rho\right) + G_i K_1\left(\kappa_i\rho\right)\right)^*\rho d\rho \\ &\qquad\qquad 1 \le i \le n, r_0 = 0 \end{aligned} \tag{42}$$

where a unit of length of conductor is considered. This integral involves product terms of I_1, K_1 Bessel functions and their corresponding conjugated values. These integrals are not directly available in the specific mathematical handbooks [23] and not have been found in other related papers. However, this referenced book includes some equivalences which can be used to solve these integrals. These equivalences are the following:

$$\begin{aligned} &\text{ber}_\nu u + j\text{bei}_\nu u = e^{\frac{1}{2}\nu\pi j} I_\nu\left(e^{\frac{\pi}{4}j}u\right) = e^{\frac{1}{2}\nu\pi j} I_\nu\left(\sqrt{j}u\right) \\ &\text{ker}_\nu u + j\text{kei}_\nu u = e^{-\frac{1}{2}\nu\pi j} K_\nu\left(e^{\frac{\pi}{4}j}u\right) = e^{-\frac{1}{2}\nu\pi j} K_\nu\left(\sqrt{j}u\right) \end{aligned} \tag{43}$$

According to these equivalences, equation (42) is rewritten as follows:

$$P_{\text{ind},i} = \frac{\pi\omega^2\sigma_i}{2}\frac{1}{\xi_i^2}\int_{\xi_i r_{i-1}}^{\xi_i r_i}(\xi_i\rho)\left[-F_i\left(\text{ber}_1(\xi_i\rho)+j\text{bei}_1(\xi_i\rho)\right)-G_i\left(\text{ker}_1(\xi_i\rho)+j\text{kei}_1(\xi_i\rho)\right)\right]$$
$$\times\left[F_i{}^*\left(\text{ber}_1(\xi_i\rho)-j\text{bei}_1(\xi_i\rho)\right)+G_i{}^*\left(\text{ker}_1(\xi_i\rho)-j\text{kei}_1(\xi_i\rho)\right)\right]d(\xi_i\rho) \tag{44}$$

where parameter ξ_i of the ith layer was defined in (13). Coefficients F_i, G_i are complex and therefore:

$$\begin{aligned} F_i &= \text{Re}(F_i)+j\text{Im}(F_i) \\ G_i &= \text{Re}(G_i)+j\text{Im}(G_i) \end{aligned} \tag{45}$$

Substituting the coefficients F_i, G_i and the Bessel functions as they appear in (44) by the values given in (43) and (45) and operating, it results four different kinds of integrals involving product terms of ber, bei, ker, and kei functions. These integrals and their solutions are the following:

$$\text{In1}_i = |F_i|^2\frac{1}{\xi_i^2}\int_{\xi_i r_{i-1}}^{\xi_i r_i}(\xi_i\rho)\left[\text{ber}_1^2(\xi_i\rho)+\text{bei}_1^2(\xi_i\rho)\right]d(\xi_i\rho) =$$
$$-|F_i|^2\frac{1}{\xi_i^2}\frac{x}{\sqrt{2}}\left[\text{ber}_1(x)\,\text{ber}_2(x)+\text{bei}_1(x)\,\text{bei}_2(x)-\text{ber}_1(x)\,\text{bei}_2(x)+\text{ber}_2(x)\,\text{bei}_1(x)\right]\Big|_{x=\xi_i r_{i-1}}^{x=\xi_i r_i} \tag{46}$$

$$\text{In2}_i = |G_i|^2\frac{1}{\xi_i^2}\int_{\xi_i r_{i-1}}^{\xi_i r_i}(\xi_i\rho)\left[\text{ker}_1^2(\xi_i\rho)+\text{kei}_1^2(\xi_i\rho)\right]d(\xi_i\rho) =$$
$$-|G_i|^2\frac{1}{\xi_i^2}\frac{x}{\sqrt{2}}\left[\text{ker}_1(x)\,\text{ker}_2(x)+\text{kei}_1(x)\,\text{kei}_2(x)-\text{ker}_1(x)\,\text{kei}_2(x)+\text{ker}_2(x)\,\text{kei}_1(x)\right]\Big|_{x=\xi_i r_{i-1}}^{x=\xi_i r_i} \tag{47}$$

$$\begin{aligned} \text{In3}_i = 2\left[\text{Re}(F_i)\,\text{Re}(G_i)+\text{Im}(F_i)\,\text{Im}(G_i)\right]\frac{1}{\xi_i^2}\times & \\ \int_{\xi_i r_{i-1}}^{\xi_i r_i}(\xi_i\rho)\left[\text{ber}_1(\xi_i\rho)\left(-\text{ker}_1(\xi_i\rho)\right)-\text{bei}_1(\xi_i\rho)\,\text{kei}_1(\xi_i\rho)\right]d(\xi_i\rho) = & \\ \left[\text{Re}(F_i)\,\text{Re}(G_i)+\text{Im}(F_i)\,\text{Im}(G_i)\right]\Big\{\frac{1}{\xi_i^2}\frac{x}{\sqrt{2}}\left[\text{kei}_1(x)\left(\text{ber}_2(x)+\text{bei}_2(x)\right)+\right. & \\ \text{ker}_1(x)\left(\text{ber}_2(x)-\text{bei}_2(x)\right)-\text{ber}_1(x)\left(\text{kei}_2(x)-\text{ker}_2(x)\right)+ & \\ \left.\text{bei}_1(x)\left(\text{kei}_2(x)+\text{ker}_2(x)\right)\right]\Big\}\Big|_{x=\xi_i r_{i-1}}^{x=\xi_i r_i} & \end{aligned} \tag{48}$$

$$\begin{aligned}\mathrm{In4}_i = 2\left[\mathrm{Im}\left(F_i\right)\mathrm{Re}\left(G_i\right)+\mathrm{Re}\left(F_i\right)\mathrm{Im}\left(G_i\right)\right]\tfrac{1}{\xi_i^2}\times \\ \int_{\xi_i r_{i-1}}^{\xi_i r_i}\left(\xi_i\rho\right)\left[\mathrm{ber}_1\left(\xi_i\rho\right)\mathrm{kei}_1\left(\xi_i\rho\right)-\mathrm{bei}_1\left(\xi_i\rho\right)\mathrm{ker}_1\left(\xi_i\rho\right)\right]d\left(\xi_i\rho\right)= \\ \left[\mathrm{Im}\left(F_i\right)\mathrm{Re}\left(G_i\right)+\mathrm{Re}\left(F_i\right)\mathrm{Im}\left(G_i\right)\right]\left\{\tfrac{1}{\xi_i^2}\tfrac{x}{\sqrt{2}}\left[\mathrm{kei}_1\left(x\right)\left(\mathrm{ber}_2\left(x\right)+\mathrm{bei}_2\left(x\right)\right)-\right.\right. \\ \mathrm{kei}_1\left(x\right)\left(\mathrm{ber}_2\left(x\right)-\mathrm{bei}_2\left(x\right)\right)-\mathrm{ber}_1\left(x\right)\left(\mathrm{ker}_2\left(x\right)+\mathrm{kei}_2\left(x\right)\right)+ \\ \left.\left.\mathrm{bei}_1\left(x\right)\left(\mathrm{ker}_2\left(x\right)-\mathrm{kei}_2\left(x\right)\right)\right]\right\}\Big|_{x=\xi_i r_{i-1}}^{x=\xi_i r_i}\end{aligned} \tag{49}$$

According to the preceding results, expression (42) or (44) can be rewritten as follows:

$$P_{\mathrm{ind},i}=\frac{\pi\omega^2\sigma_i}{2}\left(\mathrm{In1}_i+\mathrm{In2}_i+\mathrm{In3}_i+\mathrm{In4}_i\right) \tag{50}$$

Moreover, the total induced losses per unit of length of the conductor correspond to the sum of the losses of layers:

$$P_{ind}=\sum_{i=1}^{n}P_{ind,i} \tag{51}$$

In many applications, the transverse magnetic field $\mathbf{H}_t$ is generated by a coil with a current amplitude I. Therefore, a proximity resistance per unit of length R_{prox} can be defined by means of:

$$P_{ind}=\frac{1}{2}R_{prox}I^2\Rightarrow R_{prox}=\frac{2P_{ind}}{I^2} \tag{52}$$

Strictly, the precedent loss model is only appropriate for the case of conductors in uniform magnetic fields. However, this loss model also provides accurate results in applications where the device generating the magnetic field is several times bigger than the conductors.

5. Verification

The set of the preceding equations was translated into MATLAB scripts because it offers versatility and an easy-to-use implementation of Bessel functions.

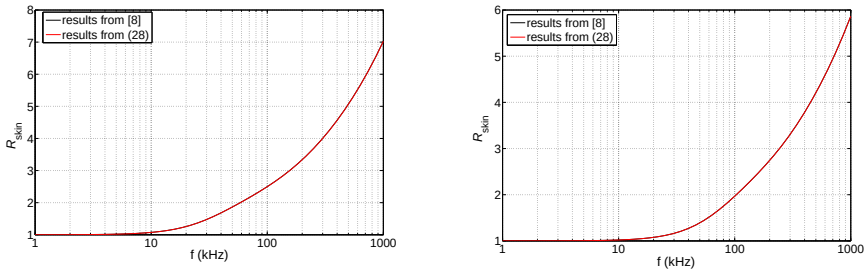

(a) (b)

Figure 3: Comparison between results of ref [8] and calculated R_{skin} of equation 28 for two-layer arrangements. (a) Bimetallic arrangement. (b) Copper tube.

It is worth remarking on some aspects of this practical implementation. First, the implementation was conveniently parameterized in order to analyze conductors with any number of layers. Second, the analytical solution of integrals (46) to (49) helps to achieve computing-time savings.

Two verifications of the model were carried out and results are reported in this section. The first verification consisted of comparing the results of Section 4 with the skin resistance model presented in [8] for bimetallic conductors. For this purposes a reference geometry consisting of two concentric layers of radii r_1=0.5 mm and r_2=1 mm was considered. Materials of layers were copper ($\sigma_1 = 5.8 \cdot 10^7 S/m, \mu_{r1} = 1$) and aluminum $\sigma_2 = 3 \cdot 10^7 S/m, \mu_{r1} = 1$), respectively. Frequency was varied from 1 kHz to 1 MHz in this verification. Real part of the equation (1) in [8] was compared with 28 for the mentioned geometry and frequency range. Results are shown in Fig. 3a. For the considered frequency range the maximum found error was 0.0517 %.

Considering that [8] is also applicable to hollow tubes, skin resistance of a copper tube with the mentioned geometry are presented in 3b. In this case the maximum found error was 0.021 %.

The developed expressions were also verified by means of a Finite Element Analysis (FEA) carried out with the ©COMSOL Multiphysics software package.

The FEA tool was configured to obtain the vector potential under the magneto-quasistatic approach (MQS), or in other words, FEA simulations were configured on the basis of 1. In order to properly capture both skin and proximity effects, a meshing strategy consisting of mapping a certain number of mesh nodes in the cable boundaries was used. The number of nodes depends on the cable radius and in this case the distance between each pair of nodes was set to $50\mu m$. Consequently, the number of elements of the mesh was independent on frequency and therefore the simulation process was simplified. The suitability of the mesh will be checked at the end of this section.

The conductor under study consisted of three layers of radii $r_1 = 0.25$ mm, $r_2 = 0.5$ mm $r_3 = 1$ mm, whose electrical conductivities were $\sigma_1 = 5.8 \cdot 10^7$ S/m, $\sigma_2 = 3 \cdot 10^7$ S/m and $\sigma_3 = 2 \cdot 10^7$ S/m, respectively. Therefore, the conductivity of the inner layer corresponds to the copper, and the conductivity of the outer layers corresponds, to some extent, to two kinds of aluminum. In this case the complete mesh consisted of 6270 elements.

Considering the skin effect, the analytical field solution and the simulated results are compared in Fig. 4. The field solution was obtained considering a voltage per unit of length of 1 V/m in the cable and the depicted current density was obtained by means of the existing relation between the current density and the potential vector shown in (11).On the other hand, FEA results were obtained by imposing a boundary condition consisting of a magnetic potential of value $-E_z/(j\omega)$ in the most external boundary of the cable. The electric field $-E_z$ corresponds to a voltage of 1 V per unit of length which is applied in the analytical solution. Fig. 4a shows the current density at 50 kHz obtained by means of the analytical model and Fig. 4b shows the results of the FEA simulations at the same frequency. Concordance between both results is checked by representing the current densities along the radial direction of the cable in the same figure. These results are shown in Fig. 4c and the accuracy achieved in this case is better than 0.025%. It is also worth to point that this error can be even improved if the node coordinates of the mesh exactly match with the evaluated point in the analytical solution.

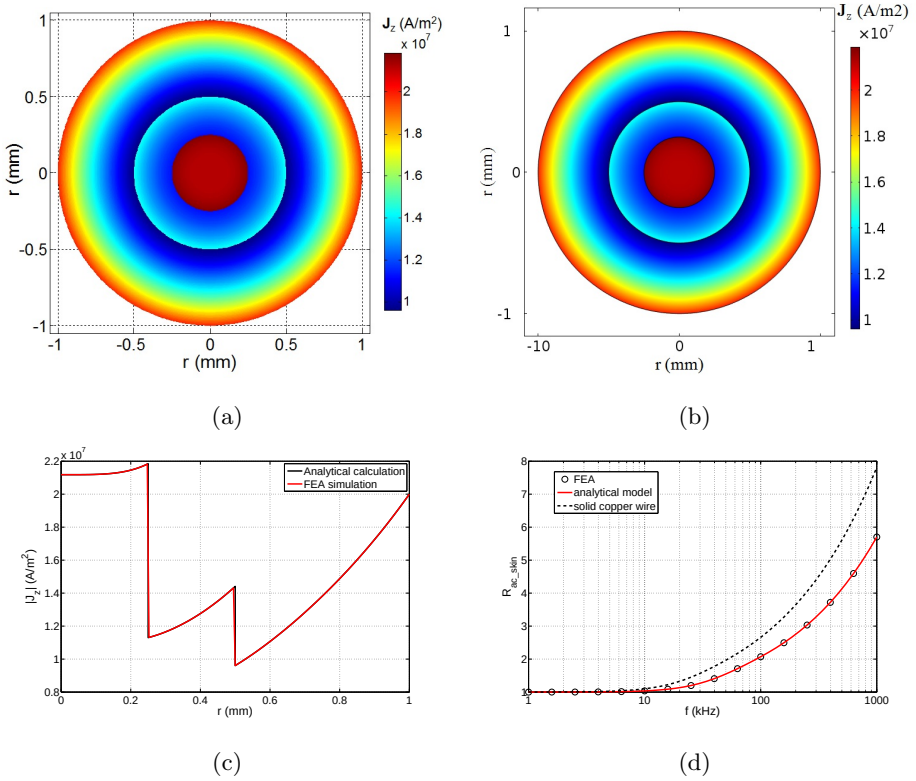

Figure 4: Current density of the conductor under a voltage of 1 V per unit of length at 50 kHz. (a) Analytical model. (b) FEA. simulations. (c) Comparison of analytical calculations and simulated results of the current density along the radial direction. (d) Comparison between the calculated and simulated R_{skin} for a frequency range comprised from 1 kHz to 1 MHz. Solid line corresponds to the analytical model. Circle marks are obtained from FEA simulations. The dashed line corresponds to R_{skin} per unit of length of a solid copper wire of diameter 2 mm diameter under the same conditions.

An additional verification has been carried out by comparing the calculated and simulated skin resistance when the frequency is changed. The results are shown in Fig. 4d. The studied frequency range is between 1 kHz and 1 MHz. The observed error between the calculated and the simulated results at the considered frquency range was lower than 0.01 %. The skin resistance of the

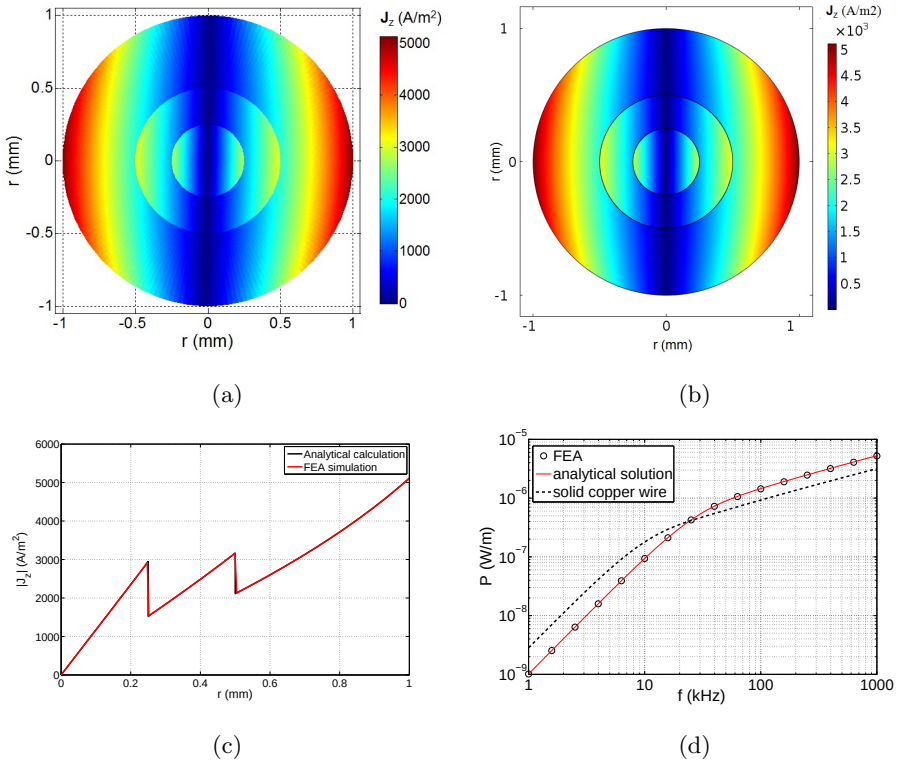

Figure 5: Induced current density in a conductor under a magnetic field of 1 A/m at 50 kHz. (a) Analytical model. (b) FEA simulations. (c) Comparison of analytical calculations and simulated results along the radial direction for $\varphi = 0$. (d) Comparison between the calculated and simulated P_{ind} for a frequency range comprised from 1 kHz to 1 MHz. Solid line corresponds to the analytical model. Circle marks are obtained from FEA simulations. The dashed line corresponds to the induced losses per unit of length of a solid copper wire of diameter 2 mm diameter under the same conditions.

multilayer conductor were also compared with the skin resistance of a solid copper wire of diameter 2 mm. Results for the solid wire are also shown in Fig. 4d by dashed line. As it is shown, the skin resistance for the multilayer conductor is lower than those of the solid copper wire at the considered frequency range.

A similar verification has been carried out for the proximity effect. In this case the multilayer conductor is under an external alternating magnetic field

of amplitude $H_t = 1$ A/m at 50 kHz. The current densities obtained from the analytical solution and FEA are shown in Fig. 5a and Fig. 5b. The boundary condition used for FEA simulations consisted of a perpendicular magnetic field of amplitude $H_t = 1$ A/m at 50 kHz. In order to apply this condition in the FEA simulations, the cable is immersed in a surrounding medium with the properties of the air. This domain was not required in the skin effect simulations. For this reason the number of mesh elements in this case is higher than the number in the previous case, exactly 28480 elements. As in the previous case, the number of elements was also independent on frequency. Induced current densities along the radial direction for $\varphi = 0$ are alse presented in Fig. 5c. In this case the observed maximum error was 0.27%.

In addition to this result, the calculated and simulated losses as a function of the frequency of the field of amplitude $H_t = 1$ A/m are also shown in Fig. 5d. The observed accuracy at the considered frequency range was better than 0.2 %. As in the previous case the proximity losses of the multilayer conductor were also compared with the proximity losses of a solid copper wire of diameter 2 mm. Results for the solid wire are also shown in Fig. 5d by dashed line. As it is shown, the proximity losses for the multilayer conductor are lower than the losses of the solid copper wire at frequencies lower than 25 kHz. This result suggests that an optimization of the conductor (number of layers, thickness and properties) could be carried out in order to minimize the losses of the windings of a specific application.

It is also worth to comment some aspects, as accuracy and computational cost of this model, with respect to the FEA tool. The same platform was used in this comparison and it consisted of a basic computer with a CPU at 2.8 GHz and 8 GB of RAM memory. The analytical model was conveniently parameterized and implemented in MATLAB.

Accuracy and computational cost of analytical and FEA are compared for different number of mesh elements at the worst case from the point of view of frequency, i.e. 1 MHz. Results are presented in Fig. 6, where the shown discrepancy results refer to resistance and dissipated power. As it is shown,

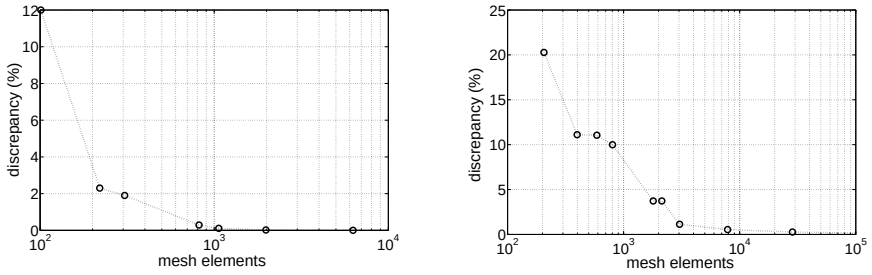

(a) (b)

Figure 6: Discrepancies between the analytical calculation and the finite element simulations. (a) Discrepancies in the resistance. (b) Discrepancies in the induced power.

discrepancies at 1 MHz are very small for a large number of mesh elements. As it was above commented, the number of mesh elements is higher in proximity effect simulations due to the surrounding media required to apply the perpendicular magnetic field.

The CPU time taken to calculate the analytical results shown in Fig. 4 was 0.055 seconds whereas the time required by the FEA tool (considering the mentioned 6270 mesh elements) was 16 seconds. Considering Fig. 5, the CPU time spent to obtain the analytical results was 0.106 seconds and the time taken by the FEA tool (with 28480 elements) was 63 seconds.

Finally, it is worth to mention some problems arising from the erratic behavior of Bessel functions for high arguments. Apart from the fact that this problem could affect any development involving Bessel functions, in this case high arguments could be reached due to the combination of high conductivity and high frequency as appear in (2). Considering copper with $\sigma_1 = 5.8 \cdot 10^7 S/m$, numerical problems arose at 17.76 MHz which is is higher than 13.56 MHz, usually considered the upper limit for induction heating or inductive power transference applications in the range of several kW.

6. Conclusions

This paper presents an analytical solution of Maxwells equations in multilayer cylindrical conductors under harmonic external electromagnetic sources. The solution is obtained in terms of the magnetic vector potential, and shows that the potential in each layer depends on the properties of the rest of the layers. The global solution is described by using a matrix approach. This solution provides the current density in each layer as well as electric and magnetic fields. The theoretical results were translated into a numerical code in which the geometry and other parameters were parameterized. The solution has been verified by means of FEA simulations.

Appendix A

Parameters of equations (17) and (36) are defined as follows:

$$K_{R_{i+1,i}} = J_1\left(k_{i+1}r_i\right)Y_0\left(k_{i+1}r_i\right) - Y_1\left(k_{i+1}r_i\right)J_0\left(k_{i+1}r_i\right) \tag{53}$$

$$R^{11}_{i+1,i} = \frac{k_i\mu_{i+1}}{\mu_i k_{i+1}}Y_0\left(k_{i+1}r_i\right)J_1\left(k_i r_i\right) - Y_1\left(k_{i+1}r_i\right)J_0\left(k_i r_i\right) \tag{54}$$

$$R^{12}_{i+1,i} = \frac{k_i\mu_{i+1}}{\mu_i k_{i+1}}Y_0\left(k_{i+1}r_i\right)Y_1\left(k_i r_i\right) - Y_1\left(k_{i+1}r_i\right)Y_0\left(k_i r_i\right) \tag{55}$$

$$R^{21}_{i+1,i} = -\frac{k_i\mu_{i+1}}{\mu_i k_{i+1}}J_0\left(k_{i+1}r_i\right)J_1\left(k_i r_i\right) + J_1\left(k_{i+1}r_i\right)J_0\left(k_i r_i\right) \tag{56}$$

$$R^{22}_{i+1,i} = -\frac{k_i\mu_{i+1}}{\mu_i k_{i+1}}J_0\left(k_{i+1}r_i\right)Y_1\left(k_i r_i\right) + J_1\left(k_{i+1}r_i\right)Y_0\left(k_i r_i\right) \tag{57}$$

$$K_{S_{i+1,i}} = 2I_1(\kappa_{i+1}r_i)K_1(\kappa_{i+1}r_i) + (\kappa_{i+1}r_i)I_1(\kappa_{i+1}r_i)K_0(\kappa_{i+1}r_i) - (\kappa_{i+1}r_i)I_0(\kappa_{i+1}r_i)K_1(\kappa_{i+1}r_i) \quad (58)$$

$$S^{11}_{i+1,i} = (\mu_{i+1}+\mu_i)K_1(\kappa_{i+1}r_i)I_1(\kappa_i r_i) + \mu_i(\kappa_{i+1}r_i)K_0(\kappa_{i+1}r_i)I_1(\kappa_i r_i) - \mu_{i+1}(\kappa_i r_i)I_0(\kappa_i r_i)K_1(\kappa_{i+1}r_i) \quad (59)$$

$$S^{12}_{i+1,i} = -(\mu_{i+1}-\mu_i)K_1(\kappa_{i+1}r_i)K_1(\kappa_i r_i) + \mu_i(\kappa_{i+1}r_i)K_0(\kappa_{i+1}r_i)K_1(\kappa_i r_i) - \mu_{i+1}(\kappa_i r_i)K_0(\kappa_i r_i)K_1(\kappa_{i+1}r_i) \quad (60)$$

$$S^{21}_{i+1,i} = -(\mu_{i+1}-\mu_i)I_1(\kappa_{i+1}r_i)I_1(\kappa_i r_i) - \mu_i(\kappa_{i+1}r_i)I_0(\kappa_{i+1}r_i)I_1(\kappa_i r_i) + \mu_{i+1}(\kappa_i r_i)I_0(\kappa_i r_i)I_1(\kappa_{i+1}r_i) \quad (61)$$

$$S^{22}_{i+1,i} = (\mu_{i+1}+\mu_i)I_1(\kappa_{i+1}r_i)K_1(\kappa_i r_i) - \mu_i(\kappa_{i+1}r_i)I_0(\kappa_{i+1}r_i)K_1(\kappa_i r_i) + \mu_{i+1}(\kappa_i r_i)I_1(\kappa_{i+1}r_i)K_0(\kappa_i r_i) \quad (62)$$

Acknowledgment

This work was partly supported by the Spanish MINECO under Project TEC2013-42937-R, Project CSD2009-00046, and Project RTC-2014-1847-6, by the DGA-FSE, by the University of Zaragoza under Project JIUZ-2014-TEC-08, and by the BSH Home Appliances Group.

References

[1] H. Dwight, Skin effect in tubular and flat conductors, Transactions of the American Institute of Electrical Engineers 37 (2) (1918) 1379–1403.

[2] H. Dwight, Skin effect and proximity effect in tubular conductors, Transactions of the American Institute of Electrical Engineers 41 (1922) 189–198.

[3] H. Dwight, A precise method of calculation of skin effect in isolated tubes, Journal of the American Institute of Electrical Engineers 42 (8) (1923) 827–831.

[4] H. Dwight, Proximity effect in wires and thin tubes, Journal of the American Institute of Electrical Engineers 42 (9) (1923) 961–970.

[5] H. Dwight, Reactance and skin effect of concentric tubular conductors, Electrical Engineering 61 (7) (1942) 513–518.

[6] A. Arnold, The alternating-current resistance of tubular conductors, Electrical Engineers, Journal of the Institution of 78 (473) (1936) 580–596. doi:10.1049/jiee-1.1936.0092.

[7] S. Schelkunoff, The electromagnetic theory of coaxial transmission lines and cylindrical shields, Bell System Technical Journal (1934) 532–578.

[8] B. Teare, J. Webb, Skin effect in bimetallic conductors, Electrical Engineering 62 (6) (1943) 297–302.

[9] K. Miller, Diffusion of electric current into rods, tubes and flat surfaces, Transactions of the American Institute of Electrical Engineers 66 (1) (1947) 1496–1502.

[10] A. Clogston, Reduction of skin-effect losses by the use of laminated conductors, Proceedings of the I.R.E. 39 (7) (1951) 767–782.

[11] H. Black, C. Mallinckrodt, S. Morgan, Experimental verification of the theory of laminated conductors, Proceedings of the IRE 40 (8) (1952) 902–905. doi:10.1109/JRPROC.1952.274095.

[12] J. Tegopoulos, E. Kriezis, Eddy current distribution in cylindrical shells of infinite length due to axial currents part i: Shells of one boundary, IEEE

Transactions on Power Apparatus and Systems PAS-90 (3) (1971) 1278–1286.

[13] V. Morgan, R. Findlay, S. Derrah, New formula to calculate the skin effect in isolated tubular conductors at low frequencies, IEE Proceedings-Science, Measurement and Technology 147 (4) (2000) 169–171.

[14] W. Mingli, F. Yu, Numerical calculations of internal impedance of solid and tubular cylindrical conductors under large parameters, IEE Proceedings-Generation, Transmission and Distribution 151 (1) (2004) 67–72.

[15] D. Filipovic, T. Dlabac, A closed form solution for the proximity effect in a thin tubular conductor influenced by a parallel filament, Serbian Journal of Electrical Engineering 7 (1) (2010) 13–20.

[16] D. Lovric, V. Boras, S. Vujevic, Accuracy of approximate formulas for internal impedance of tubular cylindrical conductors for large parameters, Progress In Electromagnetics Research M, PIER M 16 (2011) 171–184.

[17] S. Vujevic, D. Lovric, V. Boras, High-accurate numerical computation of internal impedance of cylindrical conductors for complex arguments of arbitrary magnitude, IEEE Transactions on Electromagnetic Compatibility 56 (6) (2014) 1431–1438.

[18] A. Kurs, M. Kesler, S. Johnson, Optimized design of a low-resistance electrical conductor for the multimegahertz range, Applied Physics Letters 98 (4) (2011) 172594–1–172594–4.

[19] J.A.B.Faria, Skin effect in inhomogeneous euler-cauchy tubular conductors, Progress In Electromagnetics Research M, PIER M 18 (2011) 89–101.

[20] T. A. Jankowski, N. H. Pawley, L. M. Gonzales, C. A. Ross, J. D. Jurney, Approximate analytical solution for induction heating of solid cylinders, Applied Mathematical Modelling 40 (4) (2016) 2770 – 2782. doi:http://dx.doi.org/10.1016/j.apm.2015.10.006.

[21] C. Carretero, J. Acero, R. Alonso, TM-TE decomposition of power losses in multi-stranded litz-wires used in electronic devices, Progress In Electromagnetics Research, PIER 123 (1) (2012) 83–103.

[22] E. Rothwell, M. J. Cloud, Electromagnetics, CRC Press, Boca Raton, 2001.

[23] M. Abramowitz, I. Stegun, Handbook of Mathematical Functions, Dover Publications, 1965.